J. Fluid Mech. (1984), *vol.* 149, *pp.* 455–475
Printed in Great Britain

Nonlinear stability of Newtonian fibres

By WILLIAM W. SCHULTZ, ABDELFATTAH ZEBIB,
Department of Mechanical and Aerospace Engineering, Rutgers University

STEPHEN H. DAVIS
Department of Applied Mathematics and Engineering Sciences, Northwestern University

AND YEE LEE
Owens–Corning Fiberglas Corporation, Granville, Ohio

(Received 2 September 1983 and in revised form 9 July 1984)

The stability of steady isothermal flow of one-dimensional Newtonian fibres is considered. Bifurcation theory yields a stable supercritical Hopf bifurcation, with frequency decreasing for increasing winder speeds near the critical winder speed. A new Chebyshev expansion procedure is used with time-marching to obtain accurate numerical solutions valid far from the critical point. Our numerical solution agrees well with our analytical solution near the critical winder speed, but differs significantly from those of previous numerical models. There is qualitative agreement with a previous isothermal experiment for oscillation amplitude but not for oscillation frequency. These comparisons are discussed.

1. Introduction

The manufacturing process for textile fibres consists of the extrusion of a very viscous liquid (usually molten glass or polymer) through an orifice. The resulting liquid-jet fibre is elongated by pulling it with a winder downstream of the orifice. This steady fibre flow is nearly pure elongational. For sufficiently large winder speeds this steady flow is susceptible to a hydrodynamic instability called 'draw resonance' (Petrie & Denn 1976). This instability causes time-periodic variations in the fibre diameter, which lower product performance and can disrupt the spinning process by causing fibre breakage.

In the actual process the molten fibre cools rapidly upon leaving the orifice, causing large variations in the melt viscosity. The material may also have strongly non-Newtonian rheological behaviour. However, it is widely believed (Pearson 1976) that the basic mechanism of draw resonance is retained in the simplest model of fibre-forming flow, viz the one-dimensional flow of a Newtonian fluid with constant properties and having negligible effects of air drag, inertia, surface tension and gravity.

This 'viscous-only' one-dimensional model presumes that the fibre flow varies slowly in the axial direction for both the steady flow and disturbances. This simplified model is the fundamental system studied for the past eighty years (Trouton 1906; Ziabicki 1961; Kase & Matsuo 1967; Matovich & Pearson 1969). Schultz & Davis (1982) derive these one-dimensional equations asymptotically from the axisymmetric equations of motion when 'end effects' near the orifice and winder are ignored.

The present work is a comprehensive study of the nonlinear mechanics of draw resonance. We begin by examining the weakly nonlinear behaviour of draw resonance

near critical conditions. The resulting supercritical Hopf bifurcation leads the fibre flow into a limit cycle whose angular frequency decreases with winder speed. We find a very limited range of validity of the bifurcation analysis; we estimate the range for α to extend only 0.8% above the critical value α_c, where α is the logarithm of the dimensionless winder speed.

To examine larger winder speeds we solve the full nonlinear disturbance equations numerically. We solve the initial value problem using the Crank–Nicolson method in time and a new Chebyshev expansion procedure in space (Zebib 1984). We obtain accurate representations of the strongly nonlinear oscillations for α up to 20% above α_c. We obtain good quantitative comparisons with our bifurcation theory for $\alpha \to \alpha_c$. For higher values of α we find good agreement with our results using an implicit second-order finite-difference method. We find both qualitative and major quantitative differences between our numerical simulations and those of previous workers. We also find significant differences between predictions from our model and experimental data.

2. Formulation

A slender Newtonian liquid fibre emerges from an orifice of radius r_i at an average velocity w_i into a passive gaseous environment. At a distance L the fibre is wound up at a velocity w_w as shown in figure 1. All physical properties of the liquid fibre are considered constant.

The unsteady, viscous-dominated equations were first given by Kase & Matsuo (1967). Schultz & Davis (1982) obtain these equations asymptotically from the axisymmetric equations. In non-dimensional form these are as follows:

$$(WA)_z + A_t = 0, \quad (AW_z)_z = 0, \tag{2.1a,b}$$

with

$$W(0,t) = A(0,t) = 1 \tag{2.1c,d}$$

and

$$W(1,t) = e^{\alpha} = E. \tag{2.1e}$$

Subscripts denote partial differentiation. The lengthscale is L and we use a convective timescale L/w_i. The axial velocity W and the cross-sectional area $A(=\pi R^2)$ have been made dimensionless by their values at the orifice ($z = 0$). At the winder ($z = 1$), the non-dimensional winder speed (or extension ratio) $E = w_w/w_i$ is prescribed. The natural logarithm of E is denoted by α. The continuity condition is (2.1*a*), and (2.1*b*) represents the limiting form of the Navier–Stokes equation for negligible inertia, body force and surface tension. Then (2.1*b*) states that the tensile force (viscous normal force times cross-sectional area) is constant along the fibre length. There is an exact steady-flow solution to system (2.1). This basic state is

$$A = A_s(z;\alpha) = e^{-\alpha z}, \quad W = W_s(z;\alpha) = e^{\alpha z}. \tag{2.2a,b}$$

We obtain the nonlinear disturbance equations by superposing disturbances as follows:

$$W(z,t) = W_s(z)[1 + w(z,t)], \quad A(z,t) = A_s(z)[1 + a(z,t)]. \tag{2.3a,b}$$

We have followed Pearson & Matovich (1969) in factoring W_s and A_s from the disturbances. This, in effect, scales the disturbance quantities on the local basic-state values.

If (2.3) are substituted into (2.1), we obtain the *nonlinear disturbance equations*:

$$e^{-\alpha z} a_t + a_z + w_z = -(aw)_z \quad \text{and} \quad w_{zz} - \alpha e^{-\alpha z} a_t = -(aw_z)_z, \tag{2.4a,b}$$

with

$$a(0,t) = w(0,t) = w(1,t) = 0. \tag{2.4c,d,e}$$

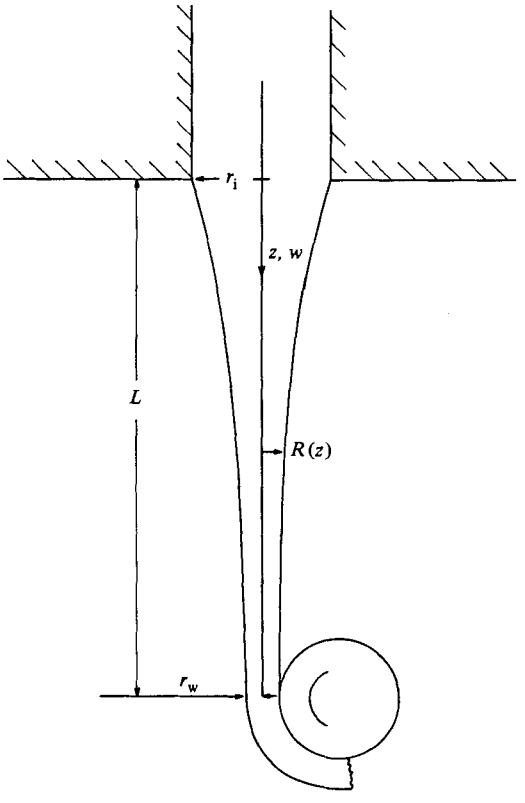

FIGURE 1. Schematic of fibre system. The orifice is located at $z = 0$ and the winder rotating at peripheral speed of w_w is located at $z = L$.

3. Bifurcation theory

It is convenient to define the vectors

$$\boldsymbol{u} = \begin{pmatrix} a \\ w \\ w_z \end{pmatrix} \quad \boldsymbol{f} = \begin{pmatrix} -(aw)_z \\ 0 \\ -(aw_z)_z \end{pmatrix} \tag{3.1a,b}$$

and write system (2.4a,b) in matrix-operator form:

$$\boldsymbol{L}'\boldsymbol{u} = \boldsymbol{f}, \tag{3.1c}$$

where $\boldsymbol{u}$ is the solution vector, $\boldsymbol{f}$ is the vector of nonlinear terms, and $\boldsymbol{L}'$ is the linear partial differential operator:

$$\boldsymbol{L}' = \begin{pmatrix} \dfrac{\partial}{\partial z} + \mathrm{e}^{-\alpha z}\dfrac{\partial}{\partial t} & 0 & 1 \\ 0 & \dfrac{\partial}{\partial z} & -1 \\ -\alpha\,\mathrm{e}^{-\alpha z}\dfrac{\partial}{\partial t} & 0 & \dfrac{\partial}{\partial z} \end{pmatrix}. \tag{3.1d}$$

The linearized stability problem $\boldsymbol{f} = \boldsymbol{0}$ yields time-periodic solutions of system (3.1) and (2.4c–e) at the critical value $\alpha = \alpha_c$ with frequency $\omega = \omega_c$. These critical values

are obtained approximately by Pearson & Matovich (1969) and Gelder (1971). We shall need to find α_c very accurately. The characteristic equation can be obtained in the form of exponential integrals (Schultz & Davis 1984), which were first written as sine and cosine integrals by Matovich & Pearson (1969). To the accuracy we require, these critical values are given by

$$\alpha_c = 3.00657, \quad \omega_c = 14.011.$$

Now we look for time-periodic solutions near the critical state. Expanding about the critical state, we have

$$\alpha = \alpha_c + \delta\alpha_1 + \delta^2\alpha_2 + \ldots, \quad \omega = \omega_c + \delta\omega_1 + \delta^2\omega_2 + \ldots, \quad \boldsymbol{u} = \delta\boldsymbol{u}_1 + \delta^2\boldsymbol{u}_2 + \ldots, \tag{3.2a,b,c}$$

where the limit-cycle amplitude δ is given by

$$\delta = \langle \boldsymbol{u}, \boldsymbol{u}_1 \rangle \equiv \int_0^{2\pi} \int_0^1 \boldsymbol{u}\cdot\boldsymbol{u}_1 \, \mathrm{d}z \, \mathrm{d}T, \tag{3.3a}$$

and T is the time scaled on the frequency by

$$T = \omega(\delta)\, t. \tag{3.3b}$$

We substitute forms (3.2) into system (3.1) and equate like powers of δ. At order δ, the linearized problem at the critical point is

$$\boldsymbol{L}''\boldsymbol{u}_1 = \boldsymbol{0}, \tag{3.4a}$$

where

$$\boldsymbol{L}'' = \begin{pmatrix} \dfrac{\partial}{\partial z} + \omega_c \, \mathrm{e}^{-\alpha_c z} \dfrac{\partial}{\partial T} & 0 & 1 \\ 0 & \dfrac{\partial}{\partial z} & -1 \\ -\alpha_c \omega_c \, \mathrm{e}^{-\alpha_c z} \dfrac{\partial}{\partial T} & 0 & \dfrac{\partial}{\partial z} \end{pmatrix}, \tag{3.4b}$$

subject to boundary conditions

$$a_1(0,t) = w_1(0,t) = w_1(1,t) = 0. \tag{3.4c,d,e}$$

and the normalization condition (3.3a) becomes

$$\langle \boldsymbol{u}_1, \boldsymbol{u}_1 \rangle = 1. \tag{3.4f}$$

We write the solutions $\boldsymbol{u}_1$ in terms of normal modes in time:

$$\boldsymbol{u}_1 = \hat{\boldsymbol{u}}_1 \, \mathrm{e}^{\mathrm{i}T} + \hat{\boldsymbol{u}}_1^* \, \mathrm{e}^{-\mathrm{i}T}, \tag{3.5a}$$

where an asterisk denotes complex conjugate. Here $\hat{\boldsymbol{u}}_1$ satisfies

$$\boldsymbol{L}_1 \hat{\boldsymbol{u}}_1 = \boldsymbol{0}, \tag{3.5b}$$

where the partial-differential operator $\boldsymbol{L}'$ has been transformed to the normal-mode operator $\boldsymbol{L}_n$:

$$\boldsymbol{L}_n = \begin{pmatrix} \mathrm{D} + \mathrm{i}n\omega_c \, \mathrm{e}^{-\alpha_c z} & 0 & 1 \\ 0 & \mathrm{D} & -1 \\ -\mathrm{i}n\omega_c \, \mathrm{e}^{-\alpha_c z} & 0 & \mathrm{D} \end{pmatrix}, \tag{3.5c}$$

where D represents differentiation with respect to z. The boundary conditions are

$$\hat{a}_1(0) = \hat{w}_1(0) = \hat{w}_1(1) = 0. \tag{3.5d,e,f}$$

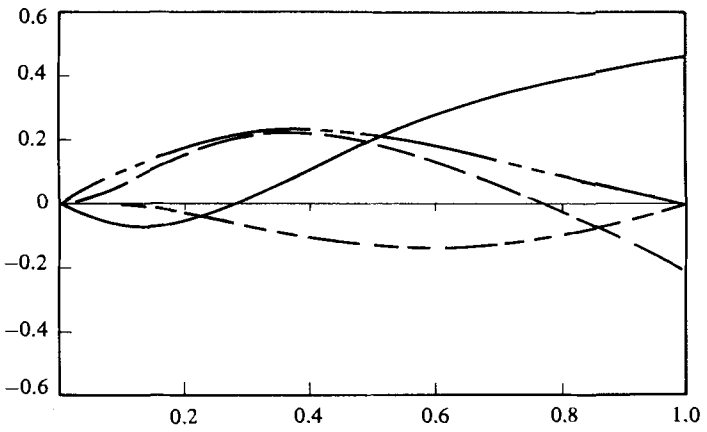

FIGURE 2. Linear solutions. The normal-mode solutions for the fibre area and velocity are given between the orifice and the winder ($z = 1$). Arbitrary phase is set by requiring $\mathrm{D}\hat{w}(0)$ to be real. ——, $\mathrm{Re}(\hat{a}_1)$; — — —, $\mathrm{Im}(\hat{a}_1)$; — — —, $\mathrm{Re}(\hat{w}_1)$; — — — —, $\mathrm{Im}(\hat{w}_1)$.

The normalization condition (3.4*f*) becomes

$$2\int_0^1 \hat{\boldsymbol{u}}_1^* \cdot \hat{\boldsymbol{u}}_1 \,\mathrm{d}z = 1 \tag{3.5g}$$

and the arbitrary phase is set by requring $\mathrm{D}\hat{w}_1(0)$ to be real. The eigen-functions at the critical point are shown in figure 2. We use a Gill-modified Runge–Kutta integrator to calculate these as well as subsequent solutions in the bifurcation analysis.

Before proceeding to higher orders, we use the inner product of (3.3*a*) to define the adjoint operator

$$\tilde{\boldsymbol{L}}'\tilde{\boldsymbol{u}} = 0, \tag{3.6a}$$

where

$$\tilde{\boldsymbol{L}}' = \begin{pmatrix} -\dfrac{\partial}{\partial z} - \omega_c \mathrm{e}^{-\alpha_c z}\dfrac{\partial}{\partial T} & 0 & \alpha_c \omega_c \mathrm{e}^{-\alpha_c z}\dfrac{\partial}{\partial T} \\ 0 & -\dfrac{\partial}{\partial z} & 0 \\ 1 & -1 & -\dfrac{\partial}{\partial z} \end{pmatrix}, \tag{3.6b}$$

with boundary conditions

$$\tilde{a}(1,T) = \tilde{w}_z(0,T) = \tilde{w}_z(1,T) = 0. \tag{3.6c,d,e}$$

We have used the nomenclature $\tilde{\boldsymbol{u}} = (\tilde{a}, \tilde{w}, \tilde{w}_z)$ to be consistent with (3.1*a*), even though $\mathrm{D}\tilde{w}$ does not equal $\tilde{w}_z$. We solve system (3.6) using normal modes. The adjoint system (3.6) also takes the form

$$\tilde{\boldsymbol{u}} = \hat{\tilde{\boldsymbol{u}}}\mathrm{e}^{\mathrm{i}T} + \hat{\tilde{\boldsymbol{u}}}^* \mathrm{e}^{-\mathrm{i}T} \tag{3.7a}$$

such that

$$\tilde{\boldsymbol{L}}\hat{\tilde{\boldsymbol{u}}} = 0, \tag{3.7b}$$

where

$$\tilde{\boldsymbol{L}} = \begin{pmatrix} -\mathrm{D} - \mathrm{i}\omega_c \mathrm{e}^{-\alpha_c z} & 0 & \mathrm{i}\alpha_c \omega_c \mathrm{e}^{-\alpha_c z} \\ 0 & -\mathrm{D} & 0 \\ 1 & -1 & -\mathrm{D} \end{pmatrix}, \tag{3.7c}$$

and subject to boundary conditions

$$\hat{\tilde{a}}(1) = \hat{\tilde{w}}_z(0) = \hat{\tilde{w}}_z(1) = 0. \tag{3.7d,e,f}$$

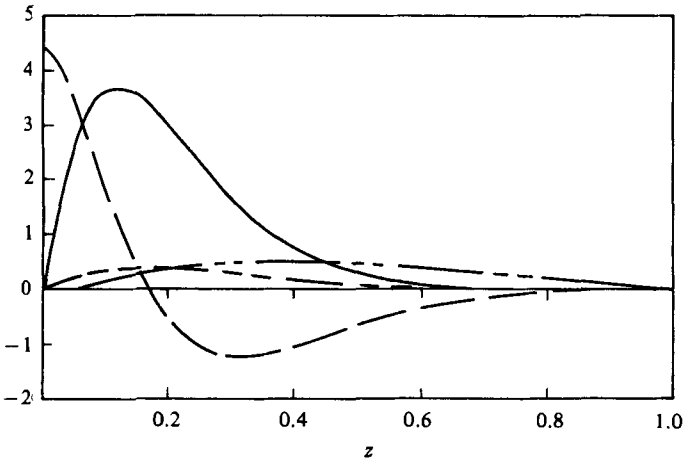

FIGURE 3. Adjoint solutions. Normalization given by $\hat{\tilde{w}}(z) = 1$. ——, $\mathrm{Re}(\hat{\tilde{a}})$; — — —, $\mathrm{Im}(\hat{\tilde{a}})$; — – —, $\mathrm{Re}(\hat{\tilde{w}}_z)$; — – – —, $\mathrm{Im}(\hat{\tilde{w}}_z)$.

The adjoint solutions are shown in figure 3, where we have used the normalization $\hat{\tilde{w}}(z) = 1$.

At order δ^2 the expansions give the system

$$\boldsymbol{L}'\boldsymbol{u}_2 = \boldsymbol{f}_2 = \begin{pmatrix} -(a_1 w_1)_z + (-\omega_1 + \alpha_1 \omega_c z)\, e^{-\alpha_c z} a_{1T} \\ 0 \\ -(a_1 w_{1z})_z + (\alpha_c \omega_1 + \alpha_1 \omega_c - \alpha_c \alpha_1 \omega_c z)\, e^{-\alpha_c z} a_{1T} \end{pmatrix}, \tag{3.8a}$$

with the boundary conditions

$$a_2(0,T) = w_2(0,T) = w_2(1,T) = 0. \tag{3.8b,c,d}$$

Since system (3.8) is inhomogeneous, we must use the Fredholm alternative theorem to guarantee solutions for $\boldsymbol{u}_2$. System (3.8) has a solution if and only if the right-hand side is orthogonal to the adjoint system, i.e. if

$$\langle \tilde{\boldsymbol{u}}, \boldsymbol{f}_2 \rangle = 0. \tag{3.9a}$$

Since the nonlinearities are quadratic, the time integration in (3.9a) always yields zero. Thus condition (3.9a) reduces to the complex equation

$$\mathrm{i}\omega_1 I_2 - \mathrm{i}\alpha_1 \omega_c I_3 = 0, \tag{3.9b}$$

where

$$I_2 = \int_0^1 (\alpha_c \hat{\tilde{w}}_z^* - \hat{\tilde{a}}^*)\, e^{-\alpha_c z} a_1 \, dz = 0.0872 - 0.0327\mathrm{i} \tag{3.9c}$$

and

$$I_3 = \int_0^1 [(\alpha_c \hat{\tilde{w}}_z^* - \hat{\tilde{a}}^*) z - \hat{\tilde{w}}_z^*]\, e^{-\alpha_c z} a_1 \, dz = 0.0145 - 0.0206\mathrm{i}. \tag{3.9d}$$

Since I_2/I_3 is not real

$$\alpha_1 = \omega_1 = 0. \tag{3.10}$$

There are no corrections to the frequency or amplitude at this order, which is the typical result for Hopf bifurcations. We solve for $\boldsymbol{u}_2$ by writing

$$u_2 = \hat{u}_{20} + \hat{u}_{20}^* + \hat{u}_{22} e^{2\mathrm{i}T} + \hat{u}_{22}^* e^{-2\mathrm{i}T}, \tag{3.11a}$$

where we have set the complementary solution to zero consistent with the $O(\delta^2)$ normalization condition $\langle \boldsymbol{u}_2, \boldsymbol{u}_1 \rangle = 0$ obtained from (3.3a). The solutions $\hat{\boldsymbol{u}}_{2n}$ satisfy

$$\boldsymbol{L}_n \hat{\boldsymbol{u}}_{2n} = \hat{\boldsymbol{f}}_{2n}, \tag{3.11b}$$

with the boundary conditions

$$\hat{a}_{2n}(0) = \hat{w}_{2n}(0) = \hat{w}_{2n}(1) = 0. \tag{3.11c,d,e}$$

Here

$$\hat{\boldsymbol{f}}_{22} = \begin{pmatrix} -\hat{a}_1 \hat{w}_{1z} - \hat{a}_{1z} \hat{w}_1 \\ 0 \\ -\hat{a}_1 \hat{w}_{1zz} - \hat{a}_{1z} \hat{w}_{1z} \end{pmatrix}, \tag{3.11f}$$

and

$$\hat{f}_{20} = \begin{pmatrix} -\hat{a}_1 \hat{w}_{1z}^* + (\mathrm{i}\omega_c \, \mathrm{e}^{-\alpha_c z} \hat{a}_1 + \hat{w}_{1z}) \hat{w}_1^* \\ 0 \\ -\hat{a}_1 (\mathrm{i}\omega_c \, \mathrm{e}^{-\alpha_c z} \hat{a}_1^*) + (\mathrm{i}\omega_c \, \mathrm{e}^{-\alpha_c z} \hat{a}_1 + \hat{w}_{1z}) \hat{w}_{1z}^* \end{pmatrix}. \tag{3.11g}$$

The functions $\hat{\boldsymbol{u}}_{20}$ and $\hat{\boldsymbol{u}}_{22}$ are given in Schultz (1982).

The corrections to the amplitude and frequency occur at order δ^3. We have

$$\boldsymbol{L}' \boldsymbol{u}_3 = \boldsymbol{f}_3 = \begin{pmatrix} -(a_1 w_2 + a_2 w_1)_z + (-\omega_2 + \alpha_2 \omega_c z) \, \mathrm{e}^{-\alpha_c z} a_{1T} \\ 0 \\ -(a_1 w_{2z} + a_2 w_{1z})_z + (\alpha_c \omega_2 + \alpha_2 \omega_c - \alpha_c \alpha_2 \omega_c z) \, \mathrm{e}^{-\alpha_c z} a_{1T} \end{pmatrix}, \tag{3.12a}$$

with the boundary conditions

$$a_3(0, T) = w_3(0, T) = w_3(1, T) = 0. \tag{3.12b,c,d}$$

The Fredholm alternative condition of system (3.13) requires

$$\langle \boldsymbol{u}, \boldsymbol{f}_3 \rangle = 0, \tag{3.13a}$$

which simplifies to

$$I_1 + \mathrm{i}\omega_2 I_2 - \mathrm{i}\alpha_2 \omega_c I_3 = 0, \tag{3.13b}$$

where

$$I_1 = \int_0^1 (\hat{\tilde{a}}_z^* g_{31} + \hat{\tilde{w}}_{zz}^* h_{31}) \, \mathrm{d}z = 0.0359 + 0.0759\mathrm{i}, \tag{3.13c}$$

$$g_{31} = \hat{a}_1 \hat{w}_{20} + \hat{a}_1^* \hat{w}_{22} + \hat{a}_{20} \hat{w}_1 + \hat{a}_{22} \hat{w}_1^* \tag{3.13d}$$

and

$$h_{31} = \hat{a}_1 \hat{w}_{20z} + \hat{a}_1^* \hat{w}_{22z} + \hat{a}_{20} \hat{w}_{1z} + \hat{a}_{22} \hat{w}_{1z}^*. \tag{3.13e}$$

We solve system (3.13) to obtain

$$\alpha_2 = 0.0350, \quad \omega_2 = -0.7892. \tag{3.13f}$$

The solution to $\hat{\boldsymbol{u}}_{31}$ provides a check on the values for α_2 and δ_2. At order δ^3 system (3.5) becomes

$$\hat{\boldsymbol{L}}_3 \boldsymbol{u}_{31} = \begin{pmatrix} -g_{31z} + \mathrm{i}(\alpha_2 z \omega_c - \omega_2) \, \mathrm{e}^{-\alpha_c z} \hat{a}_{1T} \\ 0 \\ -h_{31z} + \mathrm{i}(\alpha_c \omega_2 + \alpha_2 w_c - \alpha_c \alpha_2 z \omega_c) \, \mathrm{e}^{-\alpha_c z} \hat{a}_{1T} \end{pmatrix}, \tag{3.14a}$$

with the boundary conditions

$$\hat{a}_{31}(0) = \hat{w}_{31}(0) = \hat{w}_{31}(1) = 0. \tag{3.14b,c,d}$$

The orthogonality condition (3.13a) ensures that the boundary condition $\hat{w}_{31}(1) = 0$ is satisfied regardless of the value of the shooting parameter $\mathrm{D}\hat{w}_{31}(0)$. Schultz (1982) shows that this boundary condition is satisfied to within 0.5 %. The value of $\mathrm{D}\hat{w}_{31}(0)$ is determined from the $O(\delta^3)$ normalization condition

$$\langle \boldsymbol{u}_3, \boldsymbol{u}_1 \rangle = 0. \tag{3.14e}$$

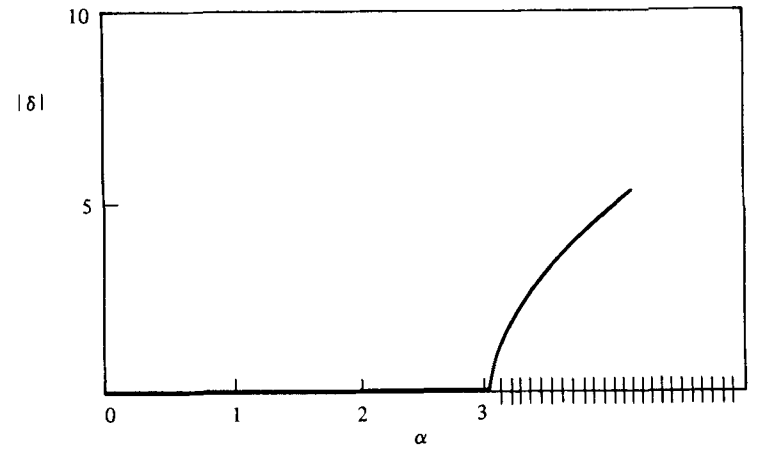

FIGURE 4. Bifurcation diagram. Unstable solutions are hatched. The branched periodic solution is represented by $|\delta|^2 = (\alpha - \alpha_c)/\alpha_2$.

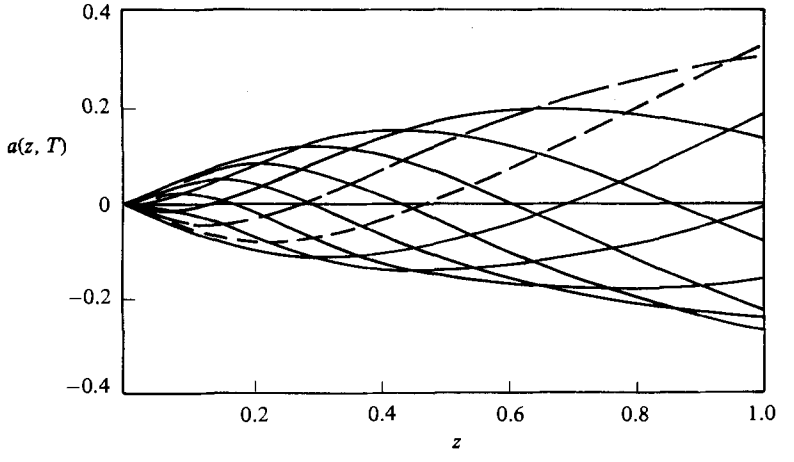

FIGURE 5. Family of solutions of $a(z, T)$ for $\alpha = 3.01$. The disturbance area at an arbitrary time is designated by a long broken line and $\frac{1}{10}$ of a period later by a short broken line. All other curves are at $\frac{1}{10}$ period intervals.

The other contribution at order δ^3 is $\hat{\boldsymbol{u}}_{33}$, which is a solution of the following system:

$$\boldsymbol{L}_3 \hat{\boldsymbol{u}}_{33} = \begin{pmatrix} -(\hat{a}_1 \hat{w}_{22} + \hat{a}_{22} \hat{w}_1)_z \\ 0 \\ -(\hat{a}_1 \hat{w}_{22z} + \hat{a}_{22} \hat{w}_{1z})_z \end{pmatrix}, \tag{3.15a}$$

with boundary conditions

$$\hat{a}_{33}(0) = \hat{w}_{33}(0) = \hat{w}_{33}(1) = 0. \tag{3.15b,c,d}$$

The periodic solution is stable by the Hopf (1942) stability theorem. The branch is stable near the critical point since the bifurcation is supercritical.

The draw resonance bifurcation diagram for the simple one-dimensional Newtonian fibre model is shown in figure 4. The steady solution represented by $|\delta| = 0$ is stable for $\alpha < \alpha_c$ and unstable for $\alpha > \alpha_c$. As α is increased past the critical value, the flow will follow a stable supercritical time-periodic branch since $\alpha_2 > 0$. The frequency decreases as the winder speed (or α) increases, since ω_2 is negative.

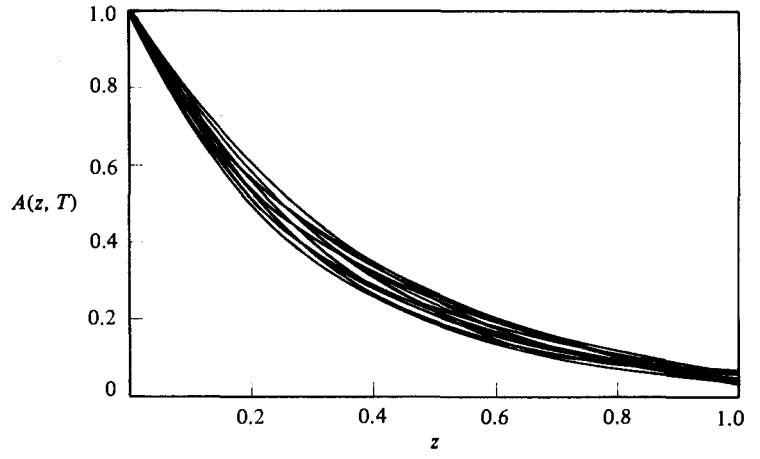

FIGURE 6. Family of solutions of $A(z, T)$ for $\alpha = 3.01$. Same as figure 5 except the areas are given as the full non-dimensional quantities using (2.3*b*).

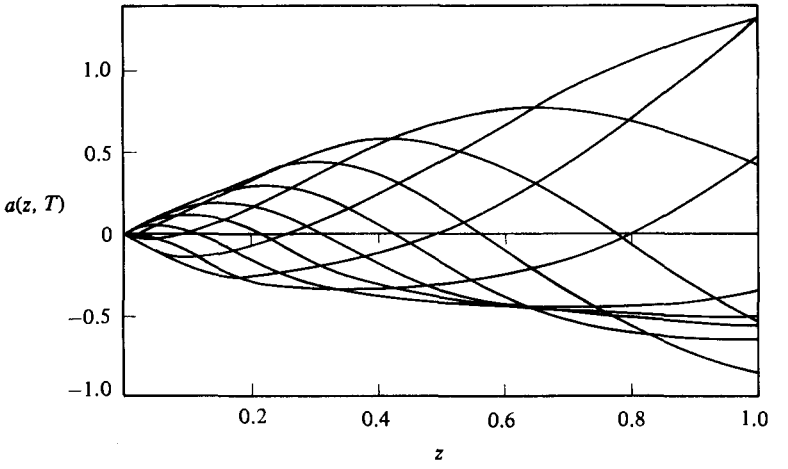

FIGURE 7. Family of solutions of $a(z, T)$ for $\alpha = 3.04$. The solutions at higher α exhibit asymmetry about $a = 0$.

Plots of $a(z, T)$ can now be drawn for extension ratios close to the critical conditions. Figures 5 and 6 show families of cross-sectional area curves for $\alpha = 3.01$ for times drawn $\frac{1}{10}$ of a period apart. The slight asymmetry about $a = 0$ is introduced by higher-order terms. Note that even at this value slightly above the critical α_c of 3.00657, the variations of the area at the winder are about 30%. The wavelike character of the disturbance is now revealed, showing that waves travel downstream with increasing speed near the winder. For the linear case, the wave speed is the velocity of the basic state $W = e^{\alpha z}$ (Schultz & Davis 1984).

As α is increased further, the higher-order terms become important and the $a(z, T)$ curves are more asymmetric, as shown in figure 7. This indicates that the weakly nonlinear theory is starting to fail. Of course, the theory must fail when negative fibre cross-sectional areas are predicted (i.e. when $a(z, T) < -1$). Based on this criteria, the present weakly nonlinear theory (to order δ^3) is valid in the narrow range $3.00657 < \alpha < 3.03$, i.e. from $\alpha = \alpha_c$ to $\alpha = 1.008\,\alpha_c$.

N	α_c	ω_c
12	3.0065544	14.010991
14	3.0065698	14.011085
16	3.0065728	14.011093

TABLE 1. Linear stability results.

α	N	Δt	a_{max}	a_{min}	ω
3.04	12	0.01	1.48	−0.647	13.30
3.04	14	0.01	1.41	−0.632	13.34
3.04	16	0.01	1.40	−0.628	13.34
3.1	16	0.01	3.02	−0.816	12.42
3.1	16	0.005	3.14	−0.830	12.34
3.1	18	0.01	2.96	−0.809	12.44
3.1	18	0.005	3.08	−0.823	12.36
3.15	20	0.01	4.17	−0.867	11.88
3.15	20	0.005	4.36	−0.882	11.74
3.15	22	0.01	4.10	−0.860	11.92
3.15	22	0.005	4.33	−0.881	11.76
3.15	22	0.0025	4.37	−0.885	11.74
3.2	20	0.01	5.47	−0.905	11.38
3.2	20	0.005	5.70	−0.916	11.24
3.2	22	0.01	5.34	−0.896	11.44
3.2	22	0.005	5.64	−0.917	11.24
3.2	22	0.0025	5.66	−0.919	11.22
3.5	20	0.005		inner divergence	
3.5	20	0.0025	16.9	−0.989	8.95
3.5	22	0.01		inner divergence	
3.5	22	0.005	15.7	−0.989	9.22
3.5	22	0.0025	15.4	−0.990	9.22
3.5	22	0.00125	15.2	−0.990	9.23
3.5	22	0.0005	15.1	−0.991	9.23
3.5	24	0.0025	14.6	−0.986	9.37
3.5	24	0.001	14.4	−0.989	9.38
3.5	26	0.001	14.1	−0.986	9.41
3.5	26	0.0005	14.1	−0.986	9.41

TABLE 2. Nonlinear limit-cycle oscillations.

The results of the bifurcation analysis do not change qualitatively when gravity, surface tension and inertia are included. When these effects are small, the values of α_c and ω_c change without affecting the values of α_2 and ω_2 (Schultz 1982).

4. Numerical solution

We now seek numerical solutions to the full strongly nonlinear initial boundary-value problem (2.4). The nonlinear system has been studied previously by Ishihara & Kase (1975) and Fisher & Denn (1975). We use a Crank–Nicolson method to march in time and a modified Galerkin–Chebyshev procedure to represent the spatial dependence of $a(z,t)$ and $w(z,t)$.

The Chebyshev representation has infinite-order convergence, and the modifications

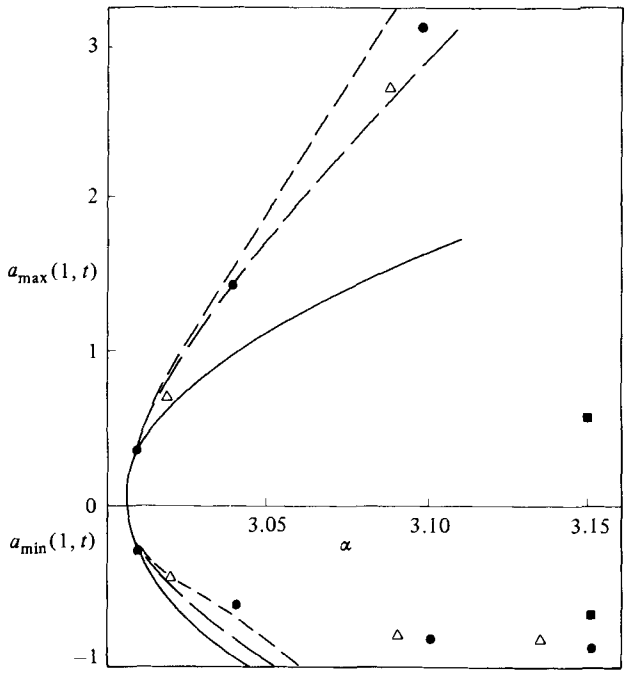

FIGURE 8. A comparison of analytical and numerical results. The bifurcation values for $a_{min}(1,t)$ and $a_{max}(1,t)$ are given by ——, — — and – – – for one-, two- and three-term expansions respectively. The results of our Chebyshev expansion numerical results are given by circles. Squares show the results of Fisher & Denn (1975) and the triangles give finite-difference results, which we use to confirm our Chebyshev expansion computations.

as presented in Zebib (1984) allow the solution to be solved as accurately as the standard tau method (Orszag 1971), but with fewer coefficients. The basis of this modification is the expansion of the highest spatial derivatives. These expansions are then integrated and the constants of integration are used to satisfy boundary conditions. The details of the numerical procedure are given in Appendix A.

Linear stability results are readily obtained from (A 10) by neglecting the quadratic nonlinearities and solving the algebraic eigenvalue problem

$$\sum_{j=0}^{N}\left[\frac{2}{\alpha}L_{kj}+\sum_{i=0}^{N}L_{ki}\,W_{ij}^{(1)}\right]w_j=\frac{-4}{\alpha\sigma}w_k \quad (0\leqslant k\leqslant N) \tag{4.1}$$

where σ are the perturbation growth rates. The results in table 1 confirm the values of α_c and ω_c. Nine significant figures of the critical values are obtained for a truncation of $N = 16$.

The initial conditions we use for $a_i(t)$ and $w_i(t)$ in the Crank–Nicolson marching technique are either the most-unstable eigenvectors of (4.1) (suitably normalized) or previously computed limit-cycle values.

At this point we abandon the norm as computed by (3.3*a*) and use instead the minimum and maximum fibre area at the winder to quantify the disturbance amplitude. These values allow direct comparisons with previous studies, and they are more informative in determining the acceptability of a man-made textile product. The maximum and minimum values of $a(1,t)$ (obtained by quadratic interpolation between time steps) as well as the oscillation frequency (a_{max}, a_{min} and ω respectively) for the limit cycles are given in table 2 for $\alpha = 3.04$, 3.1, 3.15, 3.2 and 3.5.

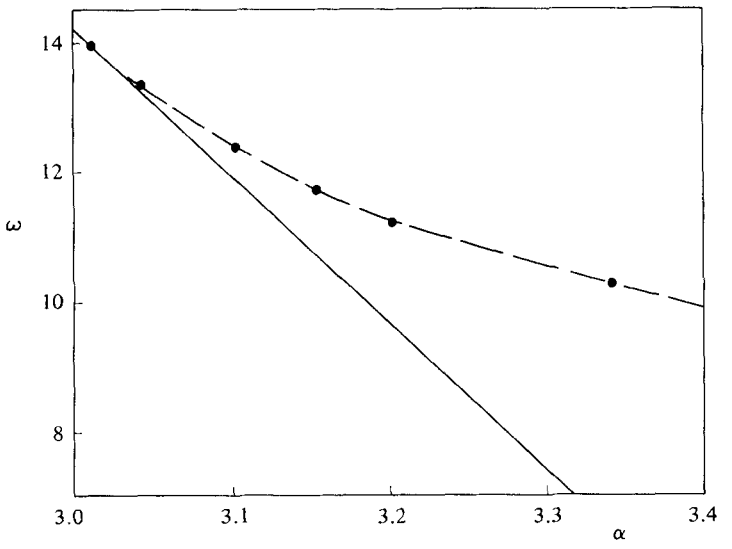

FIGURE 9. A comparison of oscillation frequency of the bifurcation analysis (——) and Chebyshev expansion results (— —).

The rapidity of the onset of strongly nonlinear behaviour is clearly indicated by our results in table 2. At the 'modestly' supercritical value $\alpha = 3.5$ we find that the maximum jet area at the winder is over 1000 times the minimum value of $1-0.986$. The period $2\pi/\omega$ of the nonlinear oscillations increases from 0.448 at the onset of draw resonance to 0.668 at $\alpha = 3.5$.

The most accurate computations of table, 2, along with another computation at $\alpha = 3.01$ using a modified linearized marching technique (see below), are compared with the bifurcation analysis in figures 8 and 9. The computed value of $a_{\max}(1, T)$ for $\alpha = 3.01$ differs by 13% from the one-term asymptotic expansion ($\boldsymbol{u} \sim \delta \boldsymbol{u}_1$) and by 1.5% from the three-term expansion ($\boldsymbol{u} \sim \delta \boldsymbol{u}_1 + \delta^2 \boldsymbol{u}_2 + \delta^3 \boldsymbol{u}_3$). The corresponding errors for $a_{\min}$ $(1, T)$ are 16 and 0.7% respectively. Computed frequencies and amplitudes asymptotically approach those of the bifurcation analysis as $\alpha \to \alpha_c$.

The fibre area at the winder ($z = 1$) is shown as a function of time for $\alpha = 3.01$, 3.1, 3.5 in figure 10. The sharp waveforms shown in figure 10 indicate that flow properties vary in the axial direction more and more rapidly as α increases. The range of validity of the one-dimensional model (2.1) becomes smaller when the disturbances cause large temporal or axial variations of the jet velocity or cross-sectional area. Clearly, for fixed slenderness ratio (orifice radius divided by the jet length) as defined by Schultz & Davis (1982), α and hence the disturbances can become sufficiently large to invalidate the one-dimensional theory.

Three criteria affect the numerical results: the Chebyshev truncation, the time step and the convergence criteria. Table 2 shows that improving the spatial resolution (increasing N) usually decreases the absolute value of $a_{\max}$, $a_{\min}$ and $1/\omega$, while improving the time resolution (decreasing Δt) has the opposite effect. The appropriate

FIGURE 10. Numerical computations of $a(1, t)$ at $\alpha = 3.01$ (a), 3.1 (b), 3.5 (c). Time origins are set by $a(1, 0) = 0$. The nearly sinusoidal pattern of $\alpha = 3.01$ becomes like the 'pulse train' at $\alpha = 3.5$ as described in Ishihara & Kase (1975). The secondary oscillations at $\alpha = 3.5$ are only found using high-resolution computations.

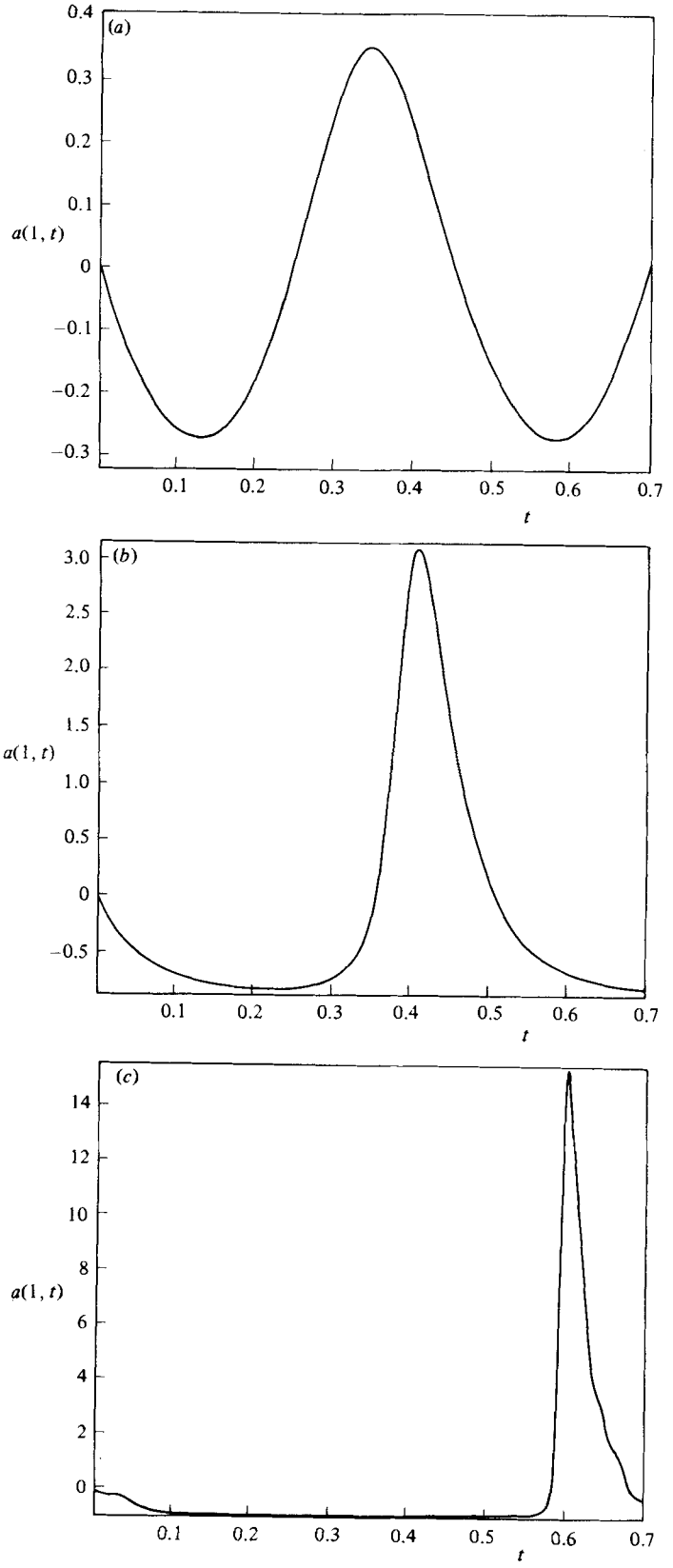

FIGURE 10. For caption see opposite.

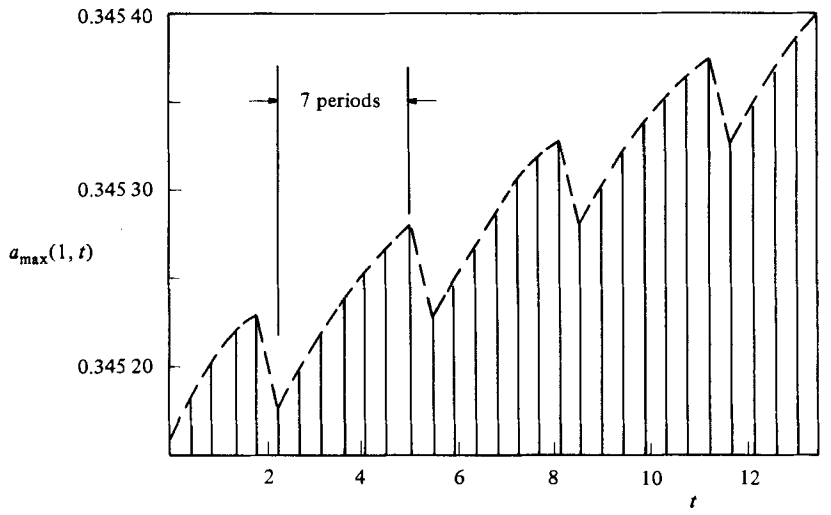

FIGURE 11. Envelope $a_{max}(1, t)$ for $\alpha = 3.01$. The maxima of $a(1, t)$ as computed with $N = 14$ and $\Delta t = 0.01$ are shown as vertical lines. The dashed envelope of these maximum show a small portion of the growth towards the limit cycle. This growth is oscillatory owing to numerical instabilities.

time step and truncation are dependent on the value of α. 'Rupture' occurs if $a = -1$. As this limit is approached, divergence of the inner iterations occurs at 'large' values of Δt. However, decreasing the time step leads to a successful march to a limit cycle. It is easily seen from figure 10 that better spatial and temporal resolution are required as α is increased and these profiles approach the 'pulse-train' profile first shown in Ishihara & Kase (1975). However, our plot of $a(1, T)$ shows secondary peaks within the limit cycle. These oscillations cannot be observed unless an implicit marching scheme is used in conjunction with high spatial representation. The strongly nonlinear nature of the results are revealed by rapid departure from the sinusoidal temporal oscillations predicted by weakly nonlinear theory.

The third factor affecting the numerical results is the set of criteria for convergence to a steady limit cycle. These criteria are made difficult by the very slow linear growth rates near critical conditions and by the oscillatory convergence to the limit cycle. Figure 11 shows the envelope of the maximum values of $a(1, T)$ for $\alpha = 3.01$ as the solution is approaching the limit cycle. The envelope is oscillatory owing to numerical instabilities in time marching. The oscillation can be eliminated by using an uneconomical time step of $\Delta t = 0.001$. Figure 11 also shows the very slow growth rate for the calculations with small $|\alpha - \alpha_c|$. Because of this behaviour, the criteria for determining the convergence to a steady limit cycle are rather subjective. We stop marching in time when the average maximum $a(1, T)$ is deemed accurate to within the significant digits presented in table 2. The steady limit cycle is obtained after about 4000 time steps for all cases where $\alpha \geqslant 3.1$. Smaller α require considerably more computation.

Because the method of solution is implicit, 3–5 inner iterations per time step are required for the computations performed when $\alpha > 3.1$. The AS/5 CPU time requirements are 4.4, 6.1, 8.5 and 11.0 s per time step for the truncation values 16, 18, 20 and 22 respectively.

To reduce the large computational requirements, we also linearized the algebraic system arising from the Crank–Nicolson procedure. This linearization cut the

computer requirements per time step to one-fifth. A truncation error analysis for this linearization procedure is given in Appendix B. This is an important saving for the small-α computations because these solutions have very slow growth rates. The computations for $\alpha = 3.01$ are obtained in this manner after 100000 time steps. However, this approach is limited to small values of α. Local numerical instabilities are found at $\alpha = 3.15$ with Δt as small as 0.001. Thus an iterative scheme must be used in conjunction with time marching to compute the nonlinear oscillations successfully for all but very small values of α. An average of (B 4) and (B 6) for the approximation of $(\phi\psi)^{t+\frac{1}{2}\Delta t}$ would eliminate the $(\mathrm{d}\phi/\mathrm{d}t)\,(\mathrm{d}\psi/\mathrm{d}t)$ term. This formulation was not attempted, although it may be useful if α is large.

5. Comparison previous work

Since the publication of the bifurcation analysis of §3 in Schultz (1982), Demay (1983) has independently performed a bifurcation analysis on the same model problem. Although his formulation is somewhat different from that presented here, he obtains essentially identical results.

Fisher & Denn (1975) present an approximate nonlinear analysis using an integral method. The non-dimensional frequency is 13.96 at $\alpha = 3.15$, showing the right trend. However, their amplitude computations differ from those presented here by about a factor of ten, as shown in figure 8. These results show qualitative differences as well, since they show that $|a_{\min}| > |a_{\max}|$. Fisher & Denn realize that their solution is not accurate, because $A(1,t)$ averaged over one time period is 8% less than the steady value. The discrepancy between these results and ours may be due to their application of a weakly nonlinear theory for values of α where it is no longer valid. Our results show that the region of validity of a weakly nonlinear theory is exceedingly small. (We validate that our solutions have reached a limit cycle by requiring that the integral of $a(1,T)$ over one period is zero to within the precision of the computed values.)

Ishihara & Kase (1975) use finite differences to examine supercritical draw resonance. Their results for $A(1,t)/A_s(1,t)$ versus time step are shown for several values of α in figure 12. We have calculated the non-dimensional frequency from these figures to show again that frequency decreases with increasing winder speeds. These computations also underestimate $a_{\max}(1,T)$ (for example, $a_{\max}$ for $\alpha \simeq 3.5$ is lower than our calculations by approximately a factor of four). These results are innaccurate because Ishihara & Kase use an explicit technique that is first-order accurate in space and time. We have also computed draw resonance using a *second*-order implicit finite-difference technique. We use a finer mesh and time step than Ishihara & Kase (typical resolutions are 200 spatial elements and a time step of 0.005), and obtain results much closer to our Chebyshev expansion results. These finite-difference maximum and minimum values of $a(1,t)$ are also plotted in figure 8. We estimate, based on these comparisons, that 26 Chebyshev polynomials give comparable spatial resolution to 800 finite-difference nodes.

There are no experimental data in a small neighbourhood about the critical parameter α_c, so comparisons must be made between experimental data and the numerical results in the strongly nonlinear range.

Donnelly & Weinberger (1975) experimentally examine draw resonance of isothermal Newtonian fibres. For their range of measurements they find that $\alpha_c \approx 2.8$ and that the disturbance amplitude, as defined by the norm given in figure 13, increases nearly linearly with extension ratio. Figure 13 also shows our computational results

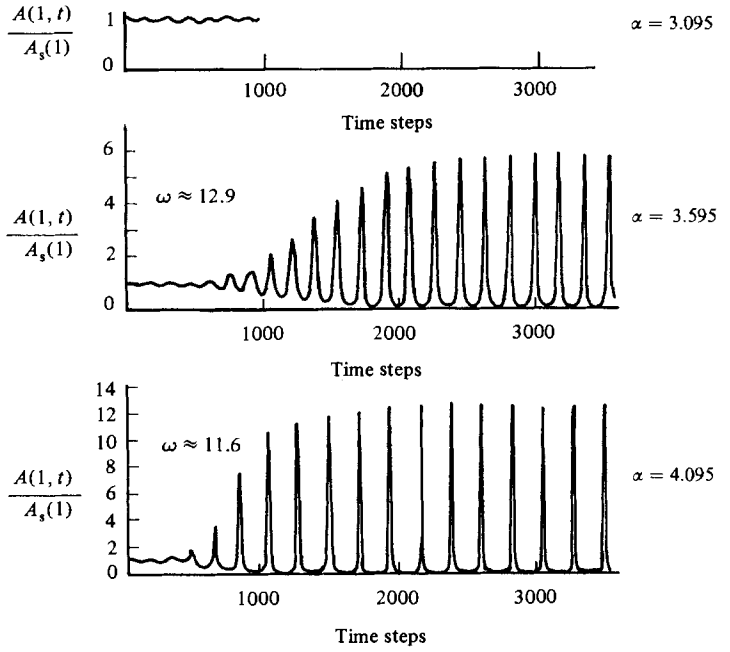

FIGURE 12. Nonlinear results of Ishihara & Kase (1975), redrawn. These solutions show the 'pulse-train' characteristic of high α. We have computed the dimensionless frequency given that a time step for these calculations is $\frac{1}{100}$ of the residence time, i.e. $\Delta t = (1-e^{-\alpha})/100\,\alpha$.

from §4 based on their norm. (Measurements are made at $z = 0.5$ and 0.25, since it is not possible to measure optically the variations in fibre area at the winder.) The caption of figure 13 gives values for the non-dimensional parameters, G, Re and Ca^{-1} (defined in Schultz & Davis 1984) governing gravitational, inertial and surface-tension forces respectively. Our present theory takes all these parameters to be zeros. Schultz (1982) shows that the values of α_2 and ω_2 remain constant for small effects of gravity, surface tension, and inertia. The data marked by triangles have large gravitational effects, and the data marked by circles have large surface-tension effects. The data given by squares most closely represents negligible gravity, surface tension and inertia. There is excellent agreement in disturbance amplitude versus extension ratio between our numerical results and experimental data for this case. It is unclear why the measured norm is unchanged between $z = 0.25$ and $z = 0.5$ for the high-gravity case marked by triangles, since an examination of a sample calculation like that shown in figure 6 shows that the norm should be a strong function of z.

Some unpublished results from the same work (C. B. Weinberger 1982 private communication) show that no perceptible change in the disturbance frequency occurs with change in amplitude, in contrast with our analytical and numerical results. (We note that the wheel diameter reported in Donnelly & Weinberger should be 63.5 mm and not 50.4 mm.) Schultz & Davis (1984) discuss the difficulties in comparing experiments with the one-dimensional model because of the end conditions near the winder and the orifice. In addition, inertia can become important in the limit-cycle oscillations even when it does not affect the steady-state flow.

Figure 14 shows fibre-weight variations for the *viscoelastic* data of Ishihara & Kase (1975). Our estimates of dimensionless frequencies from this figure show that

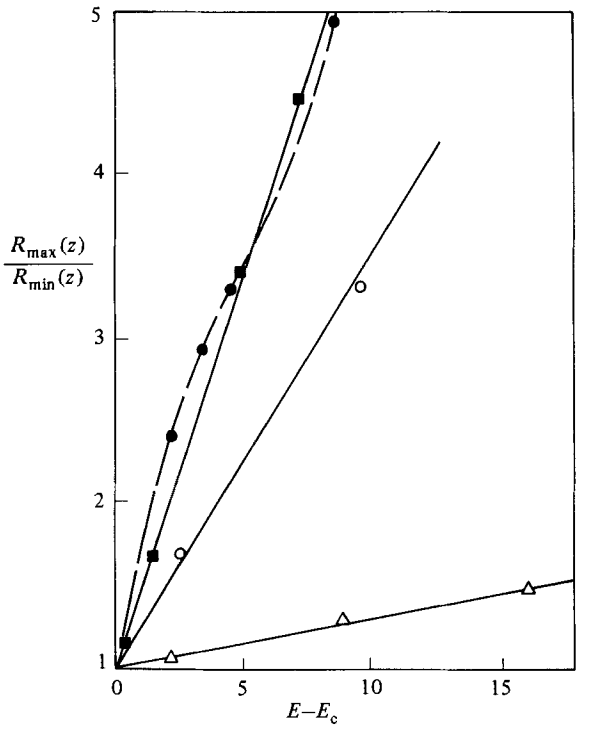

FIGURE 13. Comparison of computations with experiments. A comparison of the Chebyshev expansion results with experimental data of Donnelly & Weinberger (1975) using the norm $R_{max}(z,t)/R_{min}(z,t)$ of Donnelly & Weinberger. Here R is the free-surface radius rather than the cross-sectional area, z is fixed and t is chosen to maximize (or minimize) the jet radius over one oscillation period. The curves are forced to intersect at the origin by subtracting the critical extension ratio E_c from E. The experimental value of E_c is approximately 17, as compared with $e^{3.006\,57} = 20.21$ predicted by one-dimensional theory. Our Chebyshev computations for $z = 0.5$ are shown as a dashed line (solid circles indicate computational points). The experimental data of Donnelly & Weinberger (using the nomenclature of Schultz & Davis 1984) are given by

	G	Re	Ca^{-1}	z
■	3.75	0.0021	0.36	0.5
○	7.80	0.0010	1.71	0.5
△	31.2	0.0020	1.28	0.5, 0.25

Here G, Re and Ca^{-1} are the dimensionless groups representing gravity, inertia and surface tension respectively.

frequency *increases* rather than decreases with increasing winding speed. These wave forms show that relatively small oscillations do not have the sinusoidal pattern predicted by weakly nonlinear theory.

6. Conclusions

Our bifurcation analysis has shown formally that draw resonance is a supercritical Hopf bifurcation which leads to a limit cycle whose oscillation frequency decreases with increasing winder speeds. The analysis to leading order is valid for a very small range, $1 < \alpha/\alpha_c < 1.008$, because nonlinear terms soon dominate as $\alpha > \alpha_c$. The analysis is extended to larger α through the full numerical integration of the strongly

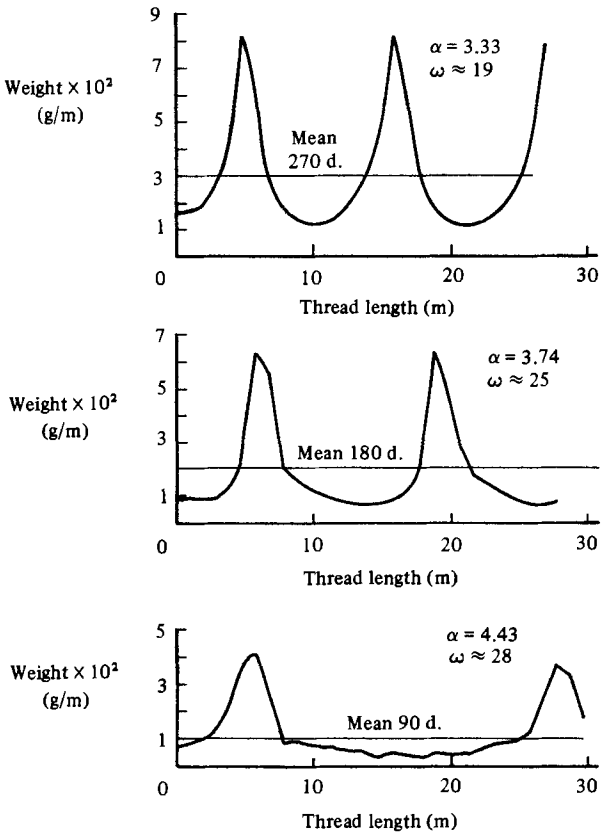

FIGURE 14. Unsteady viscoelastic experiments of Ishihara & Kase (1975), redrawn. Draw resonance of a polymer (PET) in a non-isothermal experiment is determined from measurements of the solidified fibre. Our calculations from these curves indicate that the non-dimensional frequency increases as α increases, in contrast with the isothermal Newtonian experiments, possibly indicating a new phenomenon.

nonlinear disturbance equations using a Chebyshev expansion technique. The results of these computations approach those of the bifurcation analysis as $\alpha \to \alpha_c$ and show significant differences from results of previous workers. This indicates the need for high resolution for the numerical integration of this seemingly simple nonlinear system.

Our results for oscillation amplitude as a function of winder speed compare favourably to the experimental data for isothermal, Newtonian fibres. However, there are quantitative differences in the disturbance amplitudes and the trend for the disturbance frequency has not been experimentally observed. Experiments with *viscoelastic* fluids show that frequency *decreases* with amplitude, possibly indicating a new phenomenon introduced by the material nonlinearities. Since most fibres are made from viscoelastic fluids, this would be a fruitful area for further study.

W. W. Schultz and S. H. Davis would like to acknowledge the partial support of the Owens–Corning Fiberglas Corporation. We wish to acknowledge valuable discussions with Professors G. Homsy, G. Iooss and S. Rosenblat. W. W. Schultz was also supported by Rutgers Engineering Research Council. Substantial computation time was provided by the Rutgers University Computer Service.

Appendix A

First, we use the transformation

$$x = 2z-1 \quad (-1 < x < 1). \tag{A 1}$$

Then the highest spatial derivatives of a and w in (2.4a,b) assume the representations

$$a_x = \sum_{j=0}^{N_a} a_j(t)\, T_j(x), \quad w_{xx} = \sum_{j=0}^{N_w} w_j(t)\, T_j(x), \tag{A 2a,b}$$

where $T_j(x)$ is the Chebyshev polynomial of degree j and N_a and N_w are truncation parameters. Here we have chosen $N_a = N_w = N$. For convenience in notation and algebraic manipulation we express the integrals with respect to x of (A 2) as double sums

$$a = \sum_{j=0}^{N+1}\sum_{i=0}^{N} A_{ji}\, a_i\, T_j, \quad w_x = \sum_{j=0}^{N+1}\sum_{i=0}^{N} W_{ji}^{(1)}\, w_i\, T_j \quad \text{and} \quad w = \sum_{j=0}^{N+2}\sum_{i=0}^{N} W_{ji}\, w_i\, T_j. \tag{A 3a,b,c}$$

The constant matrices A_{ji}, W_{ji} and $W_{ji}^{(1)}$ are given by

$$A_{ji} = f_{ji}^{(1)} - \delta_{j0}\,\bar{\sigma}_i \quad (0 \leqslant j \leqslant N+1), \tag{A 4a}$$

$$W_{ji}^{(1)} = f_{ji}^{(1)} - \tfrac{1}{2}\delta_{j0}(\sigma_i - \bar{\sigma}_i) \quad (0 \leqslant j \leqslant N+1), \tag{A 4b}$$

$$W_{ji} = f_{ji} - \tfrac{1}{2}\delta_{j1}(\sigma_i - \bar{\sigma}_i) - \delta_{j0}(\sigma_i + \bar{\sigma}_i) \quad (0 \leqslant j \leqslant N+2). \tag{A 4c}$$

Here f_{ji} and $f_{ji}^{(1)}$ arise from recursive relations obtained by integrating (A 2a) once and (A 2b) twice and using the identity (Orszag 1971)

$$2\,T_j = \frac{\mathrm{d}}{\mathrm{d}x}\left(\frac{c_j}{j+1}\,T_{j+1} - \frac{d_{j-2}}{j-1}\,T_{j-1}\right), \tag{A 5a}$$

where

$$c_j = d_j = 0 \quad \text{for } j < 0, \qquad c_0 = 2, \quad d_0 = 1 \quad \text{and} \quad c_j = d_j = 1 \quad \text{for } j > 0. \tag{A 5b,c,d}$$

They have the values

$$f_{ji}^{(1)} = \delta_{j,\,i+1}\, B_i^{(1)} + \delta_{j,\,i-1}\,\gamma_i^{(1)}, \quad f_{ji} = \delta_{j,\,i+1}\, B_i + \delta_{j,\,i}\,\gamma_i + \delta_{j,\,i-2}\,\delta_i, \tag{A 6a,b}$$

where $\delta_{i,\,j}$ is the Kronecker delta and the non-zero values of B_i, γ_i, and δ_i are given by

$$B_i^{(1)} = \frac{C_i}{2(i+1)}, \quad B_i = \frac{B_i^{(1)}}{2(i+2)} \quad (0 \leqslant i \leqslant N), \tag{A 6c,d}$$

$$\gamma_i^{(1)} = \frac{-1}{2(i-1)} \quad (2 \leqslant i \leqslant N), \tag{A 6e}$$

$$\gamma_i = (-B_i^{(1)} + \gamma_i^{(1)})/2i \quad (1 \leqslant i \leqslant N), \tag{A 6f}$$

$$\delta_i = \frac{-\gamma_i^{(1)}}{2(i-2)} \quad (3 \leqslant i \leqslant N). \tag{A 6g}$$

The quantities σ_i, $\bar{\sigma}_i$ and $\bar{\sigma}_i^{(1)}$ are given by

$$\bar{\sigma}_i^{(1)} = \sum_{j=0}^{N+1} f_{ji}^{(1)}, \quad \sigma_i = \sum_{j=0}^{N+2} f_{ji}, \quad \bar{\sigma}_i = \sum_{j=0}^{N+2} (-1)^j f_{ji}, \tag{A 7a,b,c}$$

chosen to satisfy the boundary conditions (2.4c–e).

The spatial dependence in (2.4) is represented by developing $e^{-\alpha z}$ in the form

$$e^{-\frac{1}{2}\alpha(1+x)} = \sum_{p=0}^{N_e} e_p T_p. \tag{A 8}$$

Rather than using the usual collocation procedure, this is obtained by solving the boundary-value problem

$$y_{xx} - \tfrac{1}{4}\alpha^2 y = 0, \quad y(-1) = 0, \quad y(1) = e^{-\alpha} \tag{A 9a,b,c}$$

by a similar expansion procedure. We find that $N_e = 12$ is sufficient to represent the exponential term to within 10^{-9} for all a considered in the range $-1 < x < 1$. We now substitute (A 1)–(A 4) in (2.4), multiply by $(1-x^2)^{-\frac{1}{2}} T_k$ and integrate over $-1 \leqslant x \leqslant 1$ to derive the initial-value problem satisfied by $a_k(t)$ and $w_k(t)$ for $0 \leqslant k \leqslant N$:

$$\frac{1}{2} \sum_{i=0}^{N} L_{ki} \dot{a}_i = -a_k - \sum_{i=0}^{N} W_{ki}^{(1)} w_i - \sum_{i=0}^{N} \sum_{j=0}^{N} N_{kij}^{(1)} a_i w_i, \tag{A 10a}$$

$$\tfrac{1}{4}\alpha \sum_{i=0}^{N} L_{ki} \dot{a}_i = w_k + \sum_{i=0}^{N} \sum_{j=0}^{N} N_{kij}^{(2)} a_i w_j, \tag{A 10b}$$

where $\cdot \equiv \mathrm{d}/\mathrm{d}t$. The expressions for L_{ki}, $N_{kij}^{(1)}$, $N_{kij}^{(2)}$ are given by

$$L_{ki} = \sum_{l=0}^{N_e} \sum_{j=0}^{N+1} B_{klj} e_l A_{ji}, \tag{A 10c}$$

$$N_{kij}^{(1)} = \sum_{l=0}^{N+2} B_{kil} W_{lj} + \sum_{l=0}^{N+1} \sum_{m=0}^{N+1} B_{klm} A_{li} W_{mj}^{(1)}, \tag{A 10d}$$

$$N_{kij}^{(2)} = \sum_{l=0}^{N+1} B_{kil} W_{lj}^{(1)} + \sum_{l=0}^{N+1} B_{klj} A_{li}, \tag{A 10e}$$

where $0 \leqslant i,j,k \leqslant N$, and the triple products are

$$B_{ikj} = \frac{2}{\pi c_i} \int_{-1}^{1} (1-x^2)^{-\frac{1}{2}} T_i T_j T_k \, \mathrm{d}k = \tfrac{1}{2}[\delta_{i,k+j} + (\delta_{i,k-j} + \delta_{i,j-k})/c_i], \tag{A 10f}$$

where we have used the identity

$$T_k T_j = \tfrac{1}{2}(T_{k+j} + T_{|k-j|}). \tag{A 10g}$$

Appendix B

The time marching of system (A 10) can be represented symbolically by

$$\frac{\mathrm{d}\zeta}{\mathrm{d}t} = \phi\psi. \tag{B 1}$$

The solution vector is represented by ζ, and $\phi\psi$ represent the quadratic nonlinear terms. A difference approximation of (B 1) is given by

$$(\zeta^{t+\Delta t} - \zeta^t)/\Delta t = (\phi\psi)^{t+\frac{1}{2}\Delta t} + O(\Delta t^2), \tag{B 2}$$

where superscripts represent the time step. The error term is given by

$$O(\Delta t^2) \sim -\frac{1}{24}\left(\frac{\mathrm{d}^3\zeta}{\mathrm{d}t^3}\right)^{t+\frac{1}{2}\Delta t} \Delta t^2 + O(\Delta t^4). \tag{B 3}$$

The Crank–Nicolson method approximates $(\phi\psi)^{t+\frac{1}{2}\Delta t}$ by the average

$$(\phi\psi)^{t+\frac{1}{2}\Delta t} = \tfrac{1}{2}[(\phi\psi)^t + (\phi\psi)^{t+\Delta t}] + O(\Delta t^2). \tag{B 4}$$

The truncation error of (B 4) is

$$O(\Delta t^2) \sim -\frac{1}{8}\left(\frac{\mathrm{d}^2\phi}{\mathrm{d}t^2}\psi + \frac{\mathrm{d}^2\psi}{\mathrm{d}t^2}\phi + 2\frac{\mathrm{d}\phi}{\mathrm{d}t}\frac{\mathrm{d}\psi}{\mathrm{d}t}\right)^{t+\frac{1}{2}\Delta t}(\Delta t^2) + O(\Delta t^4). \tag{B 5}$$

The linearized form of $(\phi\psi)^{t+\frac{1}{2}\Delta t}$ is given by

$$(\phi\psi)^{t+\frac{1}{2}\Delta t} = \tfrac{1}{2}[\phi^t\psi^{t+\Delta t} + \phi^{t+\Delta t}\psi^t] + O(\Delta t^2). \tag{B 6}$$

The truncation for the linearized formulation is then

$$O(\Delta t^2) \sim -\frac{1}{8}\left(\frac{\mathrm{d}^2\phi}{\mathrm{d}t^2}\psi + \frac{\mathrm{d}^2\psi}{\mathrm{d}t^2}\phi - 2\frac{\mathrm{d}\phi}{\mathrm{d}t}\frac{\mathrm{d}\psi}{\mathrm{d}t}\right)^{t+\frac{1}{2}\Delta t}(\Delta t^2) + O(\Delta t^4), \tag{B 7}$$

which is very similar to that of the Crank–Nicolson method.

REFERENCES

Demay, Y. 1983 Instabilité d'étirage et bifurcation de Hopf. PhD. dissertation, L'Université de Nice.

Donnelly, G. J. & Weinberger, C. B. 1975 Stability of isothermal fiber spinning of a Newtonian fluid. *Ind. Engng Chem. Fund.* **14**, 334.

Fisher, R. J. & Denn, M. M. 1975 Finite-amplitude stability and draw resonance in isothermal melt spinning. *Chem. Engng Sci.* **30**, 1129.

Gelder, G. 1971 The stability of fibre drawing processes. *Ind. Engng Chem. Fund.* **10**, 534.

Hopf, E. 1942 Bifurcation of a periodic solution from a stationary solution of a system of differential equations. English transl. (from *Berich. Math.-Phys. Kl. Sächsischen Akad. Wiss. Leipzig* **94**, 19 Jan. 1942) by L. N. Howard & N. Kopell in Marsden, J. E. & McCracken, M. *The Hopf Bifurcation and its Applications*, p. 163 (Springer, 1976).

Ishihara, H. & Kase, S. 1975 Studies of melt spinning: V. Draw resonance as a limit cycle. *J. Appl. Polymer Sci.* **19**, 557.

Kase, S. & Matsuo, T. 1967 Studies on melt spinning: II. Steady state and transient solutions of fundamental equations compared with experimental results. *J. Appl. Polymer Sci.* **11**, 251.

Matovich, M. A. & Pearson, J. R. A. 1969 Spinning a molten threadline: steady-state isothermal viscous flows. *Ind. Engng Chem. Fund.* **8**, 512.

Orszag, S. A. 1971 Galerkin approximations within slabs, spheres, and cylinders. *Phys. Rev. Lett.* **26**, 1100.

Pearson, J. R. A. 1976 Instability in non-Newtonian flow. *Ann. Rev. Fluid Mech.* **8**, 136.

Pearson, J. R. A. & Matovich, M. A. 1969 On spinning a molten threadline: stability. *Ind. Engng Chem. Fund.* **8**, 605.

Petrie, C. J. S. & Denn, M. M. 1976 Instabilities in polymer processing. *AIChE J.* **22**, 209.

Schultz, W. W. 1982 An analysis of isothermal flow of slender fibers. PhD. thesis, Northwestern University.

Schultz, W. W. & Davis, S. H. 1982 One-dimensional liquid fibers. *J. Rheol.* **26**, 331.

Schultz, W. W. & Davis, S. H. 1984 Effects of boundary conditions on the stability of slender viscous fibers. *Trans. ASME* E: *J. Appl. Mech.* **51**, 1.

Trouton, F. T. 1906 On the coefficient of viscous traction and its relation to that of viscosity. *Proc. R. Soc. Lond.* A **77**, 426.

Zebib, A. 1984 A Chebyshev method for the solution of boundary value problem. *J. Comp. Phys.* **53**, 443.

Ziabicki, A. 1961 Differential equations for velocity components in fibre spinning process. *Kolloid-Z.* **179**, 116.